Oscillations of a slider dragged on a granular bed

Antoine Dop[1,2], *Valérie* Vidal[2], and *Nicolas* Taberlet[2,*]

[1]Njord, University of Oslo, Norway
[2]LPENSL ENS Lyon – CNRS UMR 5672, Lyon, France

Abstract. We report on the emergence of an instability observed when a slider is slowly dragged across the surface of a granular bed in a quasistatic regime. The slider, designed in a boat-like shape, rests on the granular medium under its own weight and is free to move vertically and rotate around the pitch axis while being pulled at a constant horizontal speed. For a wide range of parameters—including mass, length, shape, and velocity—a regular pattern of peaks and troughs spontaneously forms as the slider moves forward. This instability is investigated through a combination of experiments using a conveyor belt setup and two-dimensional discrete element method (DEM) simulations. Our findings reveal that the wavelength and amplitude of the pattern scale with the length of the slider. Additionally, we observe that the ripples disappear for both low and high masses, suggesting the existence of an optimal confining pressure for the instability to occur.

1 Introduction

Granular materials, which are collections of discrete solid particles, exhibit a rich variety of complex behaviors that have fascinated scientists for decades. One of the most intriguing aspects of granular media is their ability to spontaneously form patterns with characteristic length scales much larger than the size of individual grains [1,2]. These patterns can arise from a variety of mechanisms, including interactions with fluid flows, external vibrations, or shear forces. For example, aeolian dunes and ripples are formed by the interaction of wind with sand grains, while underwater ripples result from the action of water currents [3,4]. Similarly, shear banding—a phenomenon where granular materials deform along narrow zones—can lead to the formation of distinct patterns under stress [5].

Another well-studied example of pattern formation in granular media is the "washboard road" instability. This phenomenon occurs when an inclined plate or wheel is repeatedly dragged or rolled over a granular surface, creating a corrugated topography with a fixed wavelength [6,7]. The washboard road instability has been observed not only in granular materials but also in other systems, such as viscoplastic fluids [8]. A key feature of this instability is that it typically requires a velocity above a certain threshold to develop. Below this critical velocity, any initial perturbations in the granular bed are erased, and no pattern forms.

In this study, we investigate a novel instability that arises when a slider is slowly pulled across a granular bed [9]. Unlike the washboard road instability, which involves repeated passages over the granular surface, our setup involves a single passage of a slider with two degrees of freedom: vertical translation and rotation around the pitch axis. This configuration results in the spontaneous formation of ripples with a well-defined wavelength. Importantly, this instability occurs in the quasistatic regime and shows no dependence on the pulling speed, distinguishing it from previously reported instabilities.

The paper is organized as follows: Section II describes the experimental setup and numerical simulation methods. Section III presents the results, focusing on the effects of the slider's mass, length, and shape on the instability. Finally, Section IV discusses the implications of these findings and the forces involved in the problem.

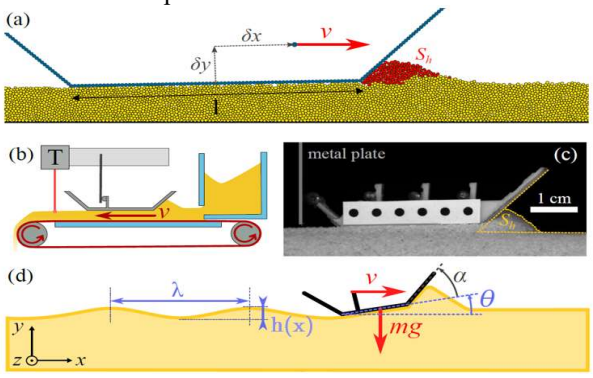

Fig. 1. (a) Snapshot of a two-dimensional discrete elements method (2D DEM) simulation [m = 0.15 g, l = 48 mm, α = 45°]. The figure only displays a small portion of the total simulation box, whose length is of about 3 m. The grains moving faster than 62.5% of v are colored in red and correspond to the heap surface S_h. (b) Sketch of the experimental setup in the threadmill configuration, with the laser telemeter T measuring the height h in the slider wake. The belt rests on a rigid horizontal plate, ensuring a flat horizontal bottom. (c) Image of the side view of the experiment displaying the heap size S_h [m = 18 g, l = 30 mm, α = 45°]. (d) Sketch of the instabilities generated by a slider over a granular bed (the real wavelength is much larger than the slider length). The slider (mass m) is pulled at a constant speed v via a rigid metallic plate. Its pitch angle is denoted θ.

* Corresponding author: nicolas.taberlet@ens-lyon.fr

2 Methods

A. Experimental Setup

The experimental setup is designed to study the instability by dragging a slider across a granular bed. To overcome the limitations of a static granular bed, we use a conveyor belt that carries a uniform layer of sand at a constant speed, v. This setup ensures a quasistatic regime, where the time for a grain to settle under its own weight is much shorter than the time it takes to be displaced horizontally by the slider by a distance equal to its diameter. Note that when an avalanche is trigged at the free surface, the motion of these grains does not remains quasistatic and inertial effect may appear in that limited region.

The granular material consists of washed natural sand with polydisperse grains of density ρ=2630±100 kg/m^3 and a mean diameter d_p=430±100 µm. The sand flows onto a 150 mm-wide conveyor belt through a rectangular slit at the bottom of a feeding tank. The belt is driven by a DC motor and gearbox to maintain a constant speed, v, and is supported by a horizontal acrylic plate to ensure a flat, stable surface.

The sliders are 3D-printed using polylactic acid (PLA) and designed with precise control over their geometry. Each slider consists of a rectangular bottom plate and two inclined plates at the front and rear. The bottom surface of the slider is covered with a monolayer of grains glued using double-sided tape to ensure grain-grain contact. The mass of the slider can be adjusted by adding steel beads, allowing us to vary the confining pressure.

A rigid metal plate pushes the slider forward via a horizontal cylinder attached to a vertical pillar. This setup ensures planar motion, preventing any roll or yaw of the slider. The slider's vertical position, y, and pitch angle, θ, are tracked using a camera, while a telemeter measures the height of the granular bed left in the slider's wake.

The details of the dimensions are given in Table 1.

Parameter	Description	Experimental	Numerical
d_p	Grain diameter	430 ± 100 μm	500 ± 100 μm
ρ_p	Grain density	$(2.63 \pm 0.1) \times 10^3$ kg.m^{-3}	1.27×10^3 kg.m^{-3} [a]
h_0	Initial thickness of the granular bed	10 mm	8.4 mm
v	Pulling speed	[1 - 100] mm/s	[1 - 1000] mm/s [b]
m	Mass of slider	[10 - 100] g	[1.25 - 25] $\times 10^{-2}$ g
l	Slider length	[30 - 100] mm	[12 - 180] mm
w	Slider width	[40 - 100] mm	d_p
P	Confining pressure	[40 - 830] Pa	[3 - 330] Pa
α	Slider spatula front angle	[30 - 60]°	[5 - 120]°
δ_x	Horizontal force position[c]	[-30 +30] mm	[-50 +50] mm
δ_y	Vertical force position[c]	[5 - 10] mm	[-20 +20] mm

Table 1. Range of parameters used in experiments and simulations.

B. Numerical Simulations

We complement our experiments with two-dimensional discrete element method (DEM) simulations. The DEM models the granular medium as a collection of deformable disks, with contact forces computed based on the relative positions and velocities of the grains as well as their history. The normal component of the contact force includes a repulsive term proportional to the overlap and a viscous damping term. The tangential component is modelled using the Cundall model, which incorporates solid friction with a memory effect [10].

The slider in the simulations is represented as a collection of grains with a diameter of $1.2d_p$. A numerical spring applies the pulling force, ensuring a constant speed. The spring (whose stiffness is chosen to avoid any noticeable stick-slip motion) is attached to a virtual point moving at a constant altitude and horizontal speed. The simulations use 100,000 grains, with six initial configurations generated for each set of parameters to account for variations in the granular bed's initial state. Table 1 shows the range of parameters used in our experiments and simulations.

3 Results

A. Observations

Figure 2 illustrates experimental and numerical examples of an instability occurring under specific parameters (explored in Secs. III.B and III.C). The panels depict the slider's altitude ($y - y_0$), wake topography ($h - h_0$), pitch angle (θ), and heap size (S_h). The instability begins from rest, with the slider initially settled under its own weight. The topography ($h - h_0$), measured post-motion, is aligned to the slider's rear corner ($x = 0$).

Despite differences between experiments (3D, rough grains) and simulations (2D, ideal disks), both exhibit similar qualitative behaviour. The instability triggers immediately upon dragging, with no transient phase. All signals show clear periodicity and correlated amplitude fluctuations, though they deviate from harmonicity—most notably in θ—due to system parameters.

Averaging over the slider's travel distance (denoted $\langle\cdot\rangle$), experiments reveal that $\langle y - y_0\rangle > 0$ due to average positive tilt $\langle\theta\rangle > 0$, while $\langle h\rangle < 0$ as grains are displaced to the sides (3D effects). In simulations, $\langle h\rangle \approx 0$ and $\langle y - y_0\rangle \approx 0$, as θ remains small. However, $\langle\theta\rangle$ is consistently positive (slider tilting upward) across all tested parameters. The heap size (S_h) behaviour differs: in simulations, it fully empties every cycle ($S_h \to 0$), whereas experiments show finite oscillations—though either scenario can occur depending on slider mass/length. Phase lags between variables vary with system properties, but the wake topography geometrically correlates with the rear corner's trajectory when contact is maintained:

$$h - h_0 = (y - y_0) - l/2 \sin\theta$$

Let us mention that near the stability threshold, intermittent oscillations may arise, with high sensitivity to initial granular bed conditions.

B. Role of the Contact Point

The relative coordinates δ_x and δ_y define the contact point where force is applied to the slider, with the origin at the center of its bottom plate (e.g., $\delta_x = -20$ mm, $\delta_y =$ 10 mm in Fig. 1c). Experiments reveal that sustained oscillations in the slider's topography occur only when pushed near its rear ($\delta_x = -20$ mm; Fig. 3a). Other δx values lead to damped oscillations. In contrast,

simulations show sustained oscillations for all tested δx, with minimal amplitude variation (Fig. 3b). This discrepancy between experiments and simulations remains unresolved.

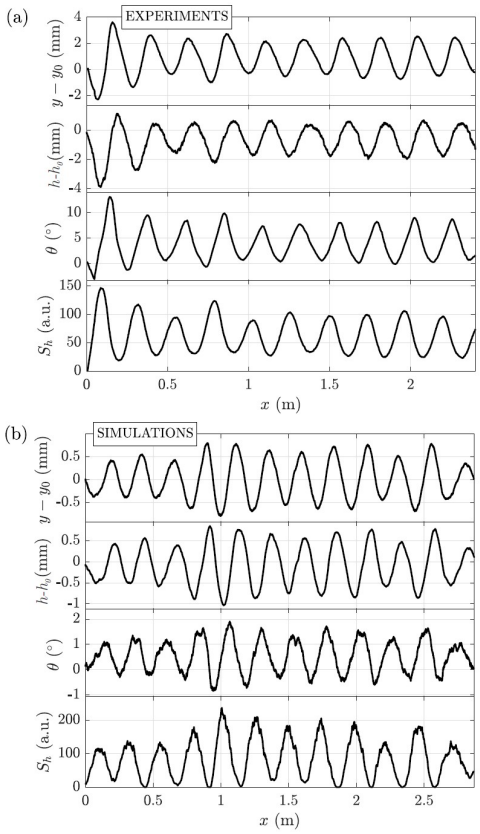

Fig. 2. Examples of surface periodic instabilities measured on the different signals. From top to bottom: slider altitude ($y-y_0$), topography ($h - h_0$) in its wake, slider pitch angle θ and plowed heap size S_h. The topography signal has been shifted to correspond to the rear corner of the slider. (a) Experimental data [m = 27 g, l = 30 mm, w = 40 mm, P = 220 Pa, α = 45°]. (b) Numerical simulation [m = 0.15 g, l = 48 mm, P = 61 Pa, α = 45°].

Figure 4 plots the oscillation amplitude against δ_x for varying δ_y, using simulations to explore impractical experimental ranges (e.g., $\delta_y < 0$, where force is applied inside the granular bed). For $\delta_y = -10$ mm, motion stabilizes—the slider tilts counterclockwise, lifting its front corner and preventing heap formation. Similarly, high δ_y tilts the slider clockwise, causing it to slide on its front spatula. Instability arises only at intermediate δ_y (null/positive), producing periodic topographies (Fig. 3b).

Intuitively, pushing from behind ($\delta_x < 0$) should destabilize (torque amplifies pitch angle), while pulling from the front ($\delta_x > 0$) should stabilize (torque corrects pitch). Experiments partially support this: $\delta_x = -20$ mm is unstable, but $\delta_x = -10$ mm is stable. Simulations, however, show instability for all δ_x when $\delta_y \geq 0$, with amplitude weakly decreasing as δ_x increases.

The time-averaged torque is positive for $\delta_y > 0$ and symmetric for $\pm\delta_x$ (slider's center of mass is mid-plate). Yet, Fig. 4 (δ_y = 20 mm, δ_x = ±50 mm) shows than opposite torques can yield unequal amplitudes. Asymmetrical mass distribution tests confirmed bias: forward weight shifts suppress oscillations, while rear shifts amplify them.

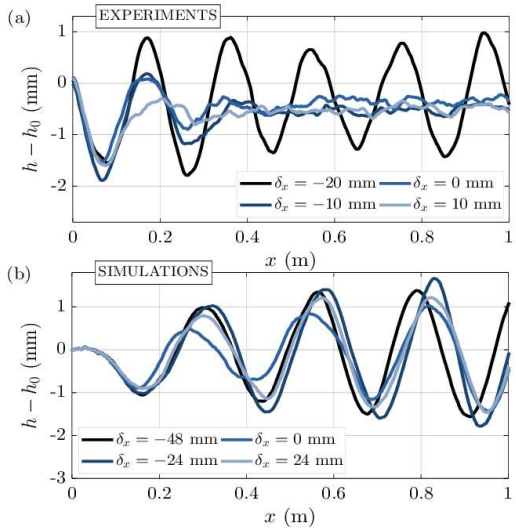

Fig. 3. Topography ($h - h_0$) as a function of the distance travelled displaying the role of the contact point horizontal coordinate δ_x in the appearance of the instability. (a) Experiments [m = 18.3 g, l = 30 mm, w = 40 mm, P = 150 Pa, α = 45°, δ_y = 10 mm]. (b) Numerical simulations [m = 0.08 g, l = 48 mm, P = 32 Pa, α = 45°, δ_y = 12 mm]. The effect of δ_x is stronger in experiments than in simulations.

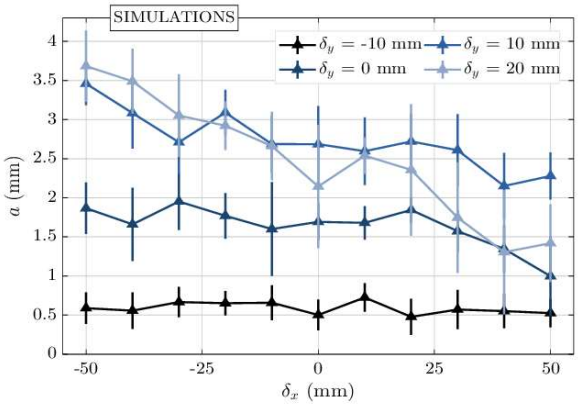

Fig. 4. Amplitude of the surface instability as a function of the horizontal location of the contact point δ_x, for different vertical position of this contact point δ_y [m = 0.08 g, l =48 mm, P = 33 Pa, α = 45°].

C. Effect of the Slider Mass and Length

Figure 5 shows the normalized wavelength (λ/l, top panels) and amplitude (a/l, bottom panels) of the slider's instability as a function of confining pressure P = mg/lw for experiments and simulations. Experimentally, increasing P raises the wavelength while reducing the amplitude. Beyond a critical pressure, the instability vanishes, and the slider moves stably (gray region in Fig. 5a), with the amplitude dropping to zero. However, even in this stable regime, a wavelength can be extracted by

perturbing the slider with a brief downward force, producing damped oscillations (red dots in Fig. 5a). These values align with the unstable regime's trend, hinting at a possible plateau, though more data are needed for confirmation.

The lightest experimental slider (m = 11 g, l = 30 mm, w = 40 mm) could not probe pressures below 90 Pa due to practical constraints (rigidity, grain layer, and added mass). Simulations, however, extended the pressure range to lower values. Figure 5b reveals that λ/l and a/l collapse onto a master curve, scaling with slider length l. At low pressures, $\lambda \approx 5l$ with minimal amplitude (~1% of l). As pressure rises, λ increases toward a plateau, while the amplitude peaks near P = 25 Pa before declining. Despite differing pressure ranges, experiments and simulations agree qualitatively: (1) amplitude decreases with higher P, and (2) wavelength grows before plateauing. This suggests an optimal confining pressure for instability.

We interpret these findings as follows: At very low P, the slider is too light to displace grains, slipping without forming a heap. Conversely, high P causes excessive grain accumulation, preventing the slider from rising, suppressing instability. The optimal pressure mirrors antlion trap dynamics, where capture probability peaks at an intermediate prey mass, linked to a friction minimum under specific pressures [11,12].

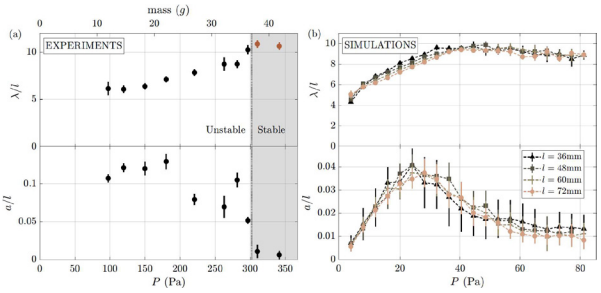

Fig. 5. Normalized wavelength λ/l (top panels) and amplitude a/l (bottom panel) of the surface instability as a function of the confining pressure. (a) Experiments. The top axis indicates the slider mass m. The red points for the wavelength in the stable regime (gray region) are obtained from damped oscillations (see text). Vertical bars indicate the error bars (when not visible, they are smaller than the dot size) [l = 30 mm w = 40 mm, α = 45°, $\delta_x = -20$ mm, $\delta_y = 10$ mm]. (b) Simulations [α = 45°, $\delta_x = 0$ mm, $\delta_y = 0$ mm].

4 Discussion

Our findings highlight the complex interplay between the slider's geometry, mass, and the mechanical properties of the granular bed. The existence of an optimal confining pressure for the instability suggests a balance between the slider's ability to plow through the grains and its tendency to rise above the surface. This behaviour is reminiscent of antlion traps, which exhibit an optimal capture probability as a function of the prey's mass.

The role of the contact point remains incompletely understood, particularly the discrepancy between experimental and numerical results. Future work should focus on refining the simulation parameters to better match experimental conditions and exploring the effects of additional degrees of freedom, such as roll and yaw.

References

1. I. S. Aranson and L. S. Tsimring, Patterns and collective behavior in granular media: Theoretical concepts, Reviews of Modern Physics 78, 641 (2006).
2. G. H. Ristow, Pattern Formation in Granular Materials, Vol. 164, Springer Science & Business Media, New York, (2000).
3. F. Charru, B. Andreotti, and P. Claudin, Sand ripples and dunes, Annual Review of Fluid Mechanics 45, 469 (2013).
4. J. F. Kennedy, The formation of sediment ripples, dunes, and antidunes, Annual Review of Fluid Mechanics 1, 147 (1969).
5. Z. Varga, V. Grenard, S. Pecorario, N. Taberlet, V. Dolique, S. Manneville, T. Divoux, G. H. McKinley, and J. W. Swan, Hydrodynamics control shear-induced pattern formation in attractive suspensions, Proceedings of the National Academy of Sciences, U.S.A. 116, 12193 (2019).
6. A.-F. Bitbol, N. Taberlet, S. W. Morris, and J. N. McElwaine, Scaling and dynamics of washboard roads, Physical Review E 79, 061308 (2009).
7. B. Percier, S. Manneville, and N. Taberlet, Modeling a washboard road: From experimental measurements to linear stability analysis, Physical Review E 87, 012203 (2013).
8. I. J. Hewitt, N. J. Balmforth, and J. N. McElwaine, Granular and fluid washboards, Journal of Fluid Mechanics 692, 446 (2012).
9. A. Dop , V. Vidal , & N. Taberlet, Surface instabilities generated by a slider pulled across a granular bed. Physical Review E,108, 024901 (2023).
10. P. A. Cundall and O. D. Strack, A discrete numerical model for granular assemblies, geotechnique 29, 4711 (1979).
11. A. Humeau, J. Rouge, and J. Casas, Optimal range of prey size for antlions, Ecological Entomology 40, 776 (2015).
12. J. Crassous, A. Humeau, S. Boury, and J. Casas, Pressure-dependent friction on granular slopes close to avalanche, Physical Review Letters 119, 058003 (2017).